C. R. Mecanique 341 (2013) 201–210

Contents lists available at SciVerse ScienceDirect

Comptes Rendus Mecanique

www.sciencedirect.com

Combustion, flow and spray dynamics for aerospace propulsion

Application of numerical simulations to predict aircraft combustor ignition

Simulations de l'allumage des foyers de chambre de combustion aéronautique

Guillaume Linassier [a,b,*], Anne Bruyat [a], Philippe Villedieu [a], Nicolas Bertier [c], C. Laurent [a], Olivier Rouzaud [a], Renaud Lecourt [d], Hubert Verdier [b], Gérard Lavergne [a]

[a] *ONERA–The French Aerospace Lab, 31055 Toulouse, France*
[b] *TURBOMECA–Safran group, 64511 Bordes cedex, France*
[c] *ONERA–The French Aerospace Lab, 92322 Châtillon, France*
[d] *ONERA–The French Aerospace Lab, 31410 Mauzac, France*

ARTICLE INFO

Article history:
Available online 16 January 2013

Keywords:
Two-phase flows
Large–Eddy simulation
Reynolds-average Navier–Stokes
Lagrangian
Combustion

Mots-clés :
Écoulements diphasiques
Simulation aux Grands Échelles
Équation de Navier–Stokes moyennée
Combustion

ABSTRACT

The present study aims at contributing to the development of a methodology to predict and improve the ignition performances of aircraft combustors. A model has been developed to investigate the early growth of a spherical ignition kernel in a two-phase flow mixture. It has been combined with a multiphysic code through two different approaches. The ignition kernel model is used to build the ignition probability map of a combustor. The output of the model can also be introduced as an initial condition in an unsteady simulation to test the flame propagation in the combustor. To validate both methods, RANS and LES simulations have been performed on an experimental combustion chamber, reproducing one sector of an industrial combustor.

RÉSUMÉ

L'objectif de cette étude est le développement d'une méthodologie permettant de prévoir l'allumage d'une chambre de combustion aéronautique. Un modèle d'allumage a été développé afin d'étudier l'expansion d'un noyau d'allumage sphérique au sein d'un brouillard. Il peut être couplé à un code de calcul CFD, et utilisé selon deux approches. La première consiste à établir une cartographie de probabilité d'allumage à partir d'un champ CFD non-réactif. La deuxième consiste à utiliser la solution du modèle comme condition initiale afin de réaliser un calcul de propagation de la flamme au foyer. Afin de valider ces deux approches, des simulations RANS et LES ont été réalisées sur une configuration de chambre de combustion équipée d'un système d'injection industriel.

1. Introduction

Spray ignition is a key parameter in the design of turbojet combustors. In case of in-flight extinction, relight must be possible, even for high altitude conditions. For helipad engines, cold engine start-up at high altitude is also necessary for

* Corresponding author at: ONERA–The French Aerospace Lab, 31055 Toulouse, France.
E-mail addresses: guillaume.linassier@onera.fr (G. Linassier), anne.bruyat@onera.fr (A. Bruyat).

1631-0721/$ – see front matter
http://dx.doi.org/10.1016/j.crme.2012.11.009

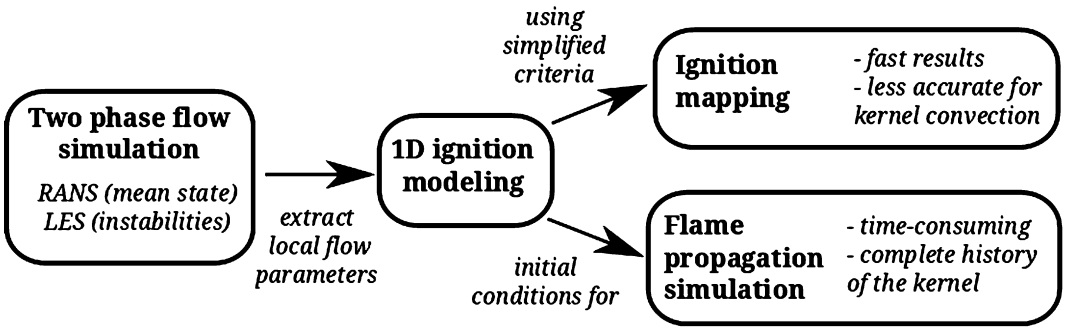

Fig. 1. Description of the ignition prediction methodology.

mountain rescue. At altitude higher than 6000 m, pressure is lower than 0.5 bar and air, engine parts as well as fuel are at temperatures as low as 233 K. These conditions are critical for engine relight, because of the degradation of spray atomization quality and vaporization process.

For air-breathing engines, the most reliable and common ignition mode is an electrical spark discharge, which efficiently converts electrical energy into a small heat deposit, with formation of radicals. The ignition process is constituted of two main phases, ignition kernel formation and kernel propagation [1]. Kernel formation can be divided into two steps: energy deposition (spark discharge) and spherical flame expansion (small-scale flame propagation). Kernel propagation also takes place in two different length scales: kernel transport into a recirculation zone, and finally flame propagation to the whole chamber.

To certify new concept of combustors, numerous and expensive ignition tests are realized over a wide range of conditions. Such tests cannot be afforded during the preliminary design phases. An alternative approach is the use of reliable numerical tools which could reduce the overall design cycle.

Nowadays, with the growth of computational performances, LES can be afforded for such purpose. LES offers the advantage to capture the large scale of turbulence, and is suitable to model a highly stochastic phenomena like ignition [2], but it still needs great computational cost. Moreover, before performing a time consuming flame propagation simulation, it should be interesting to use a simple methodology to predict ignition of the combustor [3,4].

An ignition kernel model has been developed and combined with a CFD code in two ways (see Fig. 1). Firstly, the ignition model is used to build the ignition probability map of a combustor. Secondly, an ignition simulation is introduced as initial condition in an unsteady simulation to model the complete flame propagation.

Both methodologies are tested on a mono-sector combustor, experimentally characterized on the MERCATO test-rig (ONERA–Mauzac). RANS and LES have been performed with the CFD code CEDRE. Spray has been modeled using a Lagrangian approach. Non-reactive simulations have been validated thanks to velocity fields of the two-phase flow and droplet size fields provided by LDA and PDA measurements. It has been also verified that LES captures correctly gas flow instabilities. From RANS two-phase flow field, an ignition probability map and two flame propagation simulations have been studied. Similar simulations are expected to be performed using instantaneous LES flow fields.

2. Prior ignition two-phase flow simulation

2.1. Two-phase flow solver

2.1.1. Gaseous solver

The unstructured compressible code CEDRE (ONERA) has been used for both RANS and LES, with an implicit time advancement and a second-order upwind scheme. For RANS approach, the kinetic energy is modeled by the standard k–l model, with an inlet turbulence level $u'/\bar{u}$ set to 5%. For LES, the Smagorinsky model has been used to model the subgrid turbulent scales. A non-reflecting condition was considered at the exit of the combustor.

2.1.2. Dispersed phase solver

The liquid phase is modeled using a Lagrangian approach, considering two-way coupling for liquid–gas interactions. Kerosene is represented by the surrogate specie *KERO* mentioned in Section 3.1. An infinite conductivity model was used to predict the evaporation of the droplets, and the Ranz–Marshall correlations are used to modify the Nusselt and Sherwood numbers. For RANS simulations, the turbulent dispersion is taken into account with a Langevin model. A complex treatment is applied to the walls to compute the droplets velocity and size after impact. Depending on their properties (temperature, Weber number), the droplets will bounce at the wall, or splash [5].

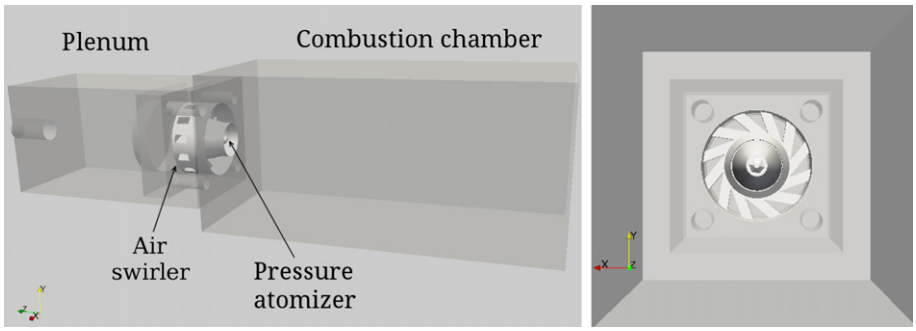

Fig. 2. Schematic view of the MERCATO combustion chamber.

2.2. Test case description

2.2.1. Geometry

The test case is a mono-sector combustor with square section (see Fig. 2). Dimensions of the combustion chamber are $129 \times 129 \times 250$ mm^3, coordinates of walls being $z = 0$ mm for the head-end one and x or $y = \pm 64.5$ mm for the lateral ones. The injection system, designed by Turbomeca, is composed of a pressure atomizer and an air swirler. The complete test-rig includes a plenum and an exhaust pipe, which are also meshed, so the flow inside the injection system is also modeled, and the boundary conditions at the inlet and the exit are well defined. A spark plug device can be mounted on the lateral wall, at four different locations ($z = 26$, 56, 86 or 116 mm).

For the present study, all simulations have been performed at atmospheric conditions, with $Q_{air} = 35.0$ g.s^{-1}, $Q_{kero} = 2.25$ g s^{-1}, $P = 1$ bar and $T = 293$ K. The global equivalence ratio Φ_l is equal to 0.95. For these operating conditions, the combustor has been thoroughly experimentally characterized on the MERCATO facility at ONERA [6].

For flame propagation, two spark plug positions have been tested, located at $z = 56$ mm and 116 mm. Ignition tests for 56 mm abscissa gave ignition with a probability $P_{ign} = 37\%$ [7]. For the 116 mm position, ignition is not possible for this global equivalence ratio.

2.2.2. Injection modeling

Fuel is injected downstream from the injector nozzle, as an ensemble of injection points distributed as concentrical rings. Injection profile is defined from particle granulometry and velocimetry measurements, obtained with a two-component PDA system at the $z = 6$ mm section. Polydisperse effects are taken into account, by injecting ten classes of droplets size with corresponding size and velocity distributions.

In the RANS case, the fuel is injected at the measurement section. With LES, injection is done at the $z = 0$ mm section, that is to say at 4 mm from the injector. This is done in order to take into account effects of the swirl on the droplets from the early instants. Granulometry is conserved, since $T = 293$ K.

2.3. Results for cold flow

2.3.1. Gaseous phase

For LES and RANS, gas velocity field has been compared to experimental data measured with a two-component LDA device (see Fig. 3). Measurements are not available for the simulated operating conditions, but previous works [6] showed that mean and RMS velocities are self-similar, and can be normalized using the air bulk velocity. For the current study, we used operating conditions for which the bulk velocity is 10% lower than the one for which measurements have been performed. For both LES and RANS, the mean velocity profiles show good agreement with the measured ones. LES approach gives better results for RMS value levels, whereas RANS tends to underestimate the kinetic turbulent energy. Same tendencies have been observed in other works on swirling flow [8].

The experimental pressure loss between plenum and the combustion chamber was measured to approximately equal $\Delta P_{exp} = 5300$ Pa. Comparison with numerical simulations shows little discrepancies, with $\Delta P_{LES} = 4500$ Pa, and $\Delta P_{RANS} = 4300$ Pa.

With a high enough bulk velocity, swirling flow exhibits a hydrodynamic instability called Precessing Vortex Core [9]. Pressur spectra were obtained using a microphone for non-reactive conditions [6]. On Fig. 4, LES and experimental pressure spectra are compared. Maximum spectral density indicates the frequency of the hydrodynamic instability, which is 930 Hz for LES and 1050 Hz for experiments. The gap encountered between these results is slight. Other frequencies are presumably related to acoustic. The structure of double-helix of the PVC can be observed from LES unsteady flow field, on Fig. 4. These results show how LES is well adapted to compute unsteady phenomena.

2.3.2. Dispersed phase

Validation of the two-phase flow is difficult, since only few experimental data on the simulation operating conditions are available. Size and velocity distributions have been measured only on the $z = 6$ mm section. Fuel flow rate can be validated

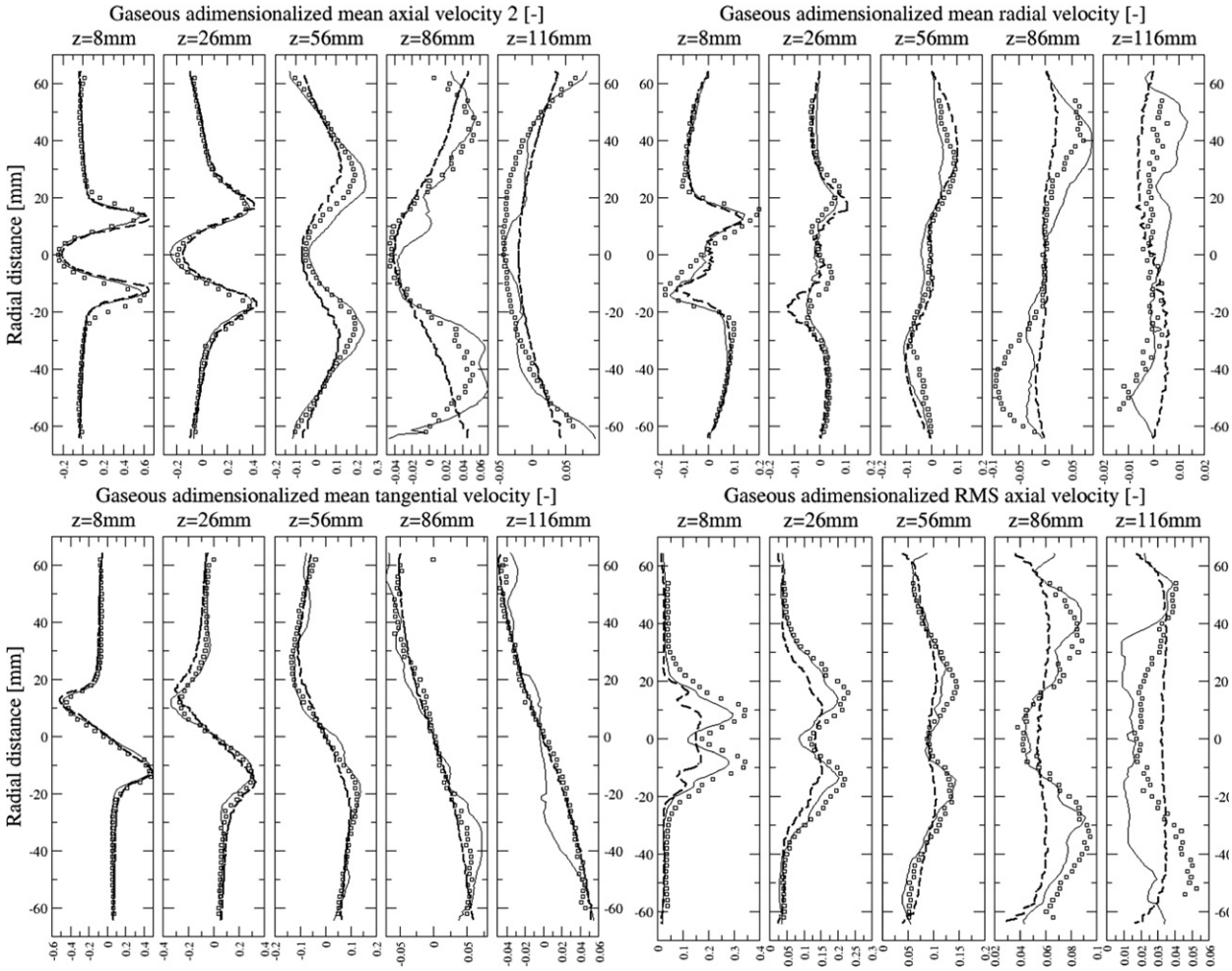

Fig. 3. Simulation of the non-reactive flow, gaseous phase (□ = LDA, – = LES, -- = RANS).

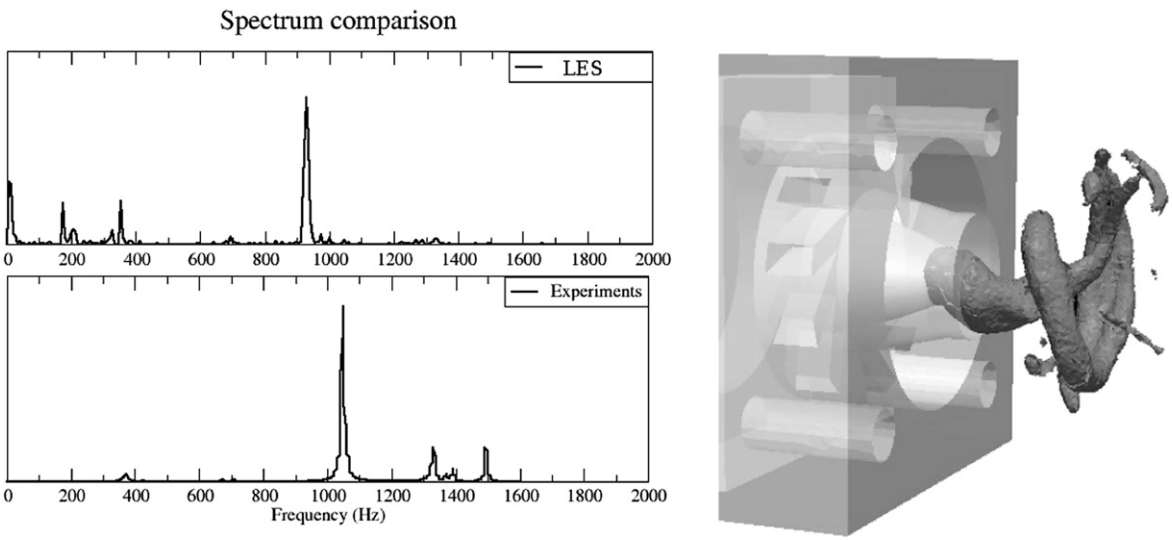

Fig. 4. Pressure spectra from LES and experiment; structure of the PVC from LES (iso-contour $P = 103\,000$ Pa).

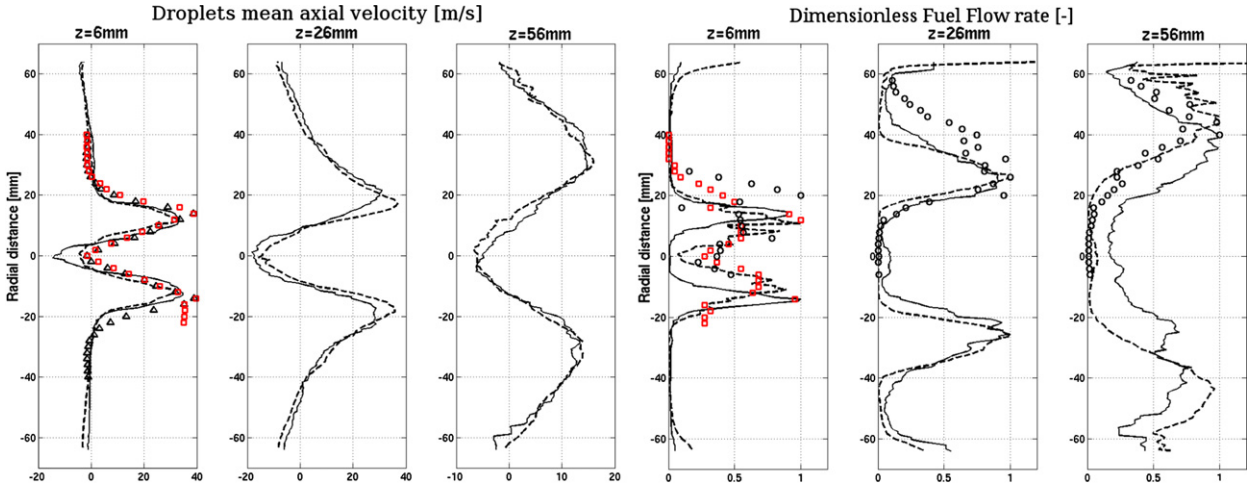

Fig. 5. Simulation of the non-reactive flow, liquid phase (□ [horizontal traverse] and △ [vertical traverse] = PDA for simulated operating conditions, – = LES, -- = RANS, ○ = PDA for similar operating conditions).

for other abscissas, using normalized measurements for similar operating conditions. It is necessary to check the spatial distribution of the spray inside the chamber. Axial droplets velocity and normalized fuel flow rate are presented on Fig. 5. For both variables, comparison between experiments and simulation showed that the behavior of the spray is correctly reproduced by RANS.

3. Ignition modeling

3.1. Ignition kernel model

The aim of the present model is to simulate the early propagation of an ignition kernel in a two-phase mixture [10]. The energy deposition is considered as an instantaneous, adiabatic and isobaric heating process, which creates a spherical laminar flame front. On the first stage of ignition, it is assumed that the flame front is not wrinkled by turbulence. With these hypotheses, the kernel growth phase is described by numerical resolution of conservation equations for 1D dilute–spray mixture. In spherical coordinates, it gives Eqs. (1), (2) and (3), with the source terms $\dot{\rho}_{i,\chi}$ and $\dot{\mathcal{H}}_{\chi}$ for chemical reactions, and $\dot{\rho}_{l,v}$ and $\dot{\mathcal{H}}_{v}$ for fuel evaporation. Droplets are described by a Lagrangian approach, with their displacement being neglected during kernel simulation.

$$\frac{\partial \rho_g}{\partial t} + \frac{1}{r^2}\frac{\partial}{\partial r}\left(r^2 \rho_g u_{r,g}\right) = \dot{\rho}_{l,v} \tag{1}$$

$$\rho_g \frac{\partial Y_i}{\partial t} + \rho_g u_{r,g}\frac{\partial Y_i}{\partial r} - \frac{1}{r^2}\frac{\partial}{\partial r}\left(r^2 \rho_g \mathcal{D}_{i,g}\frac{\partial Y_i}{\partial r}\right) = \dot{\rho}_{l,v}(\delta_{i,\mathrm{F}} - Y_i) + \dot{\rho}_{i,\chi} \tag{2}$$

$$\rho_g c_{p_g}\frac{\partial T_g}{\partial t} + \rho_g c_{p_g} u_{r,g}\frac{\partial T_g}{\partial r} - \frac{1}{r^2}\frac{\partial}{\partial r}\left(r^2 \lambda_g \frac{\partial T_g}{\partial r}\right) = \dot{\mathcal{H}}_{v} - \dot{\rho}_{l,v} h_{l,(g)} + \dot{\mathcal{H}}_{\chi} \tag{3}$$

The energy deposit takes place in a spherical volume of radius r_0, close to the spark plug air-gap. Ignition kernel simulation starts after the kernel has expanded to a radius $r_1 > r_0$. The initial radius r_1 and temperature T_1 are calculated from kernel visualization and the energy of the spark discharge. It is assumed that the total energy loss during spark generation equals 50% of the electrical energy supplied to the spark plug. The final state of the kernel is designated by r_f and T_f.

It is also assumed that the kernel expansion takes place in a quiescent mixture. In order to fulfill this hypothesis, the ignition simulation time has been set as the time necessary for the kernel to move his diameter. This time has been measured experimentally.

Combustion is modeled using a reduced two-step chemical scheme (see Eq. (4)). The chemical reaction rate is calculated with an Arrhenius law, for which a correction of the pre-exponential factor depending on the local equivalence ratio is made [11]. Fuel is modeled by a mono-component specie, referred as *KERO*.

$$KERO + 10 \cdot O_2 \rightarrow 10 \cdot CO + 10 \cdot H_2O \quad \text{and} \quad CO_2 + \frac{1}{2} \cdot O_2 \leftrightarrows CO_2 \tag{4}$$

Fig. 6 shows the laminar flame speed S_L computed with the model for a laminar flame front in purely gaseous mixture, for several pressure, temperature of unburned gas T_u and equivalence ratio Φ. Comparison with results computed with detailed chemistry shows good agreement.

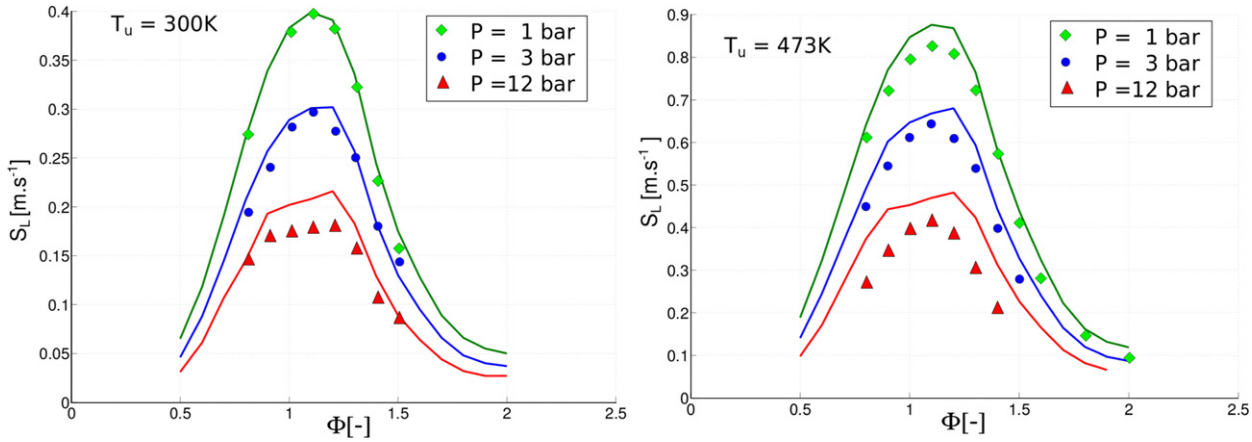

Fig. 6. Laminar flame speed computed with the ignition model (symbols) and with detailed chemistry (line).

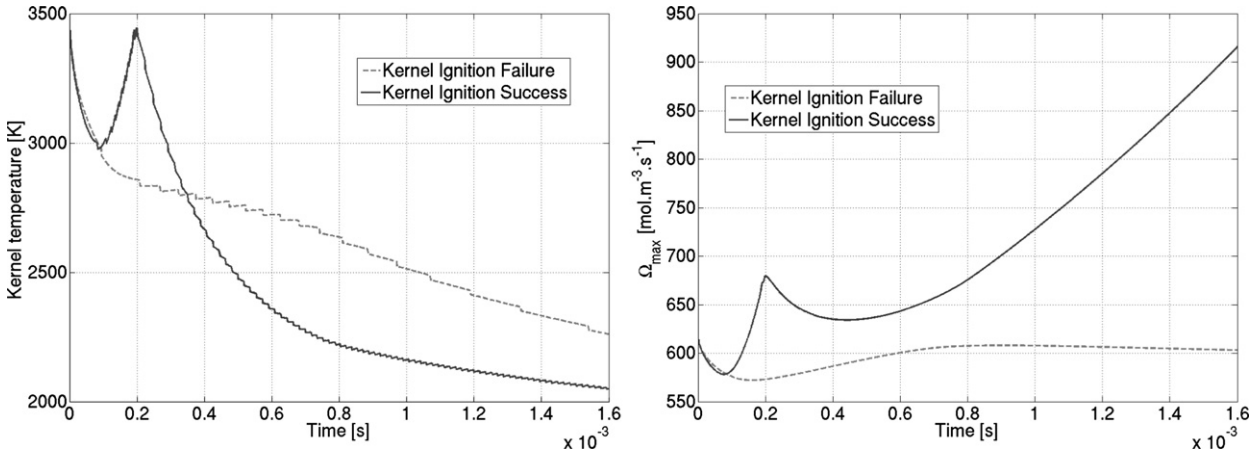

Fig. 7. Time evolution of the mean kernel temperature and of the maximum reaction rate during ignition simulation.

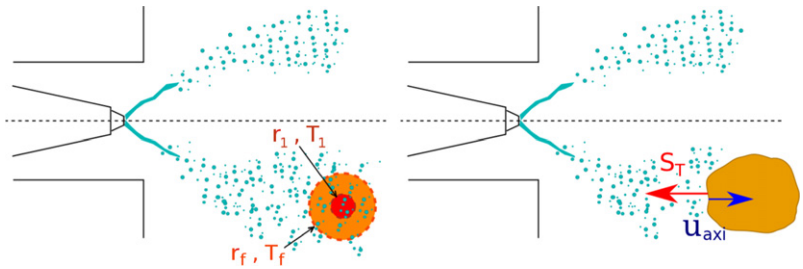

Fig. 8. Ignition mapping criteria: on the left, one-dimensional simulation of the laminar kernel growth; on the right, criteria on the flame kernel propagation to the injector nozzle.

The kernel model is used to perform quick analysis of the ignition of a combustor, from an instantaneous or mean flow field (see Fig. 8). Local ignition is tested through three criteria:

- *Condition 1*: If enough fuel vapor is produced and temperature is high enough to enable combustion, the mean kernel temperature temporal evolution shows an inflexion point (*see* Fig. 7).
- *Condition 2*: Growth of the kernel is analyzed to eliminate positions where ignition occurs, but with no flame front propagation ($r_f/r_1 \geqslant A > 1$).
- *Condition 3*: Final kernel temperature is examined to guarantee the flame front sustained ($T_f \geqslant B$).

Thresholds A and B can be adjusted to eliminate more or less spark discharge locations.

3.2. Ignition mapping

If the three conditions for local ignition are fulfilled, the propagation of the flame to the injector is predicted using a simplified criterion (*Condition 4*), based on the comparison of the turbulent flame speed S_T to the axial velocity component u_{axi}:

(i) $S_T > u_{axi}$: the kernel is advected toward the injector, and the flame spreads to the whole combustor,
(ii) $S_T \leqslant u_{axi}$: the kernel is advected toward the combustor exit, and the ignition is not possible.

with the turbulent flame speed S_T, calculated for a stoechiometric gaseous mixture like $S_T = S_L^0 + u'$ [12]. From RANS turbulent variables, the upstream propagation probability of the kernel $P_{up} = P(S_T > u_{axi})$ can be computed at the energy deposit location. With the assumption that u' follows a normal law, P_{up} can be expressed as in Eq. (5). This is not sufficient to describe the complex trajectory of the kernel, but it can be used to discriminate locations where upstream flame propagation is not possible.

$$P_{up} = \int_0^{+\infty} \frac{1}{u'\sqrt{2\pi}} \cdot e^{-\frac{1}{2}\left(\frac{x - S_T + \overline{u_{axi}}}{u'}\right)^2} \cdot \mathrm{d}x = \frac{1}{2} \cdot \left(erfc\left(\frac{-S_T + \overline{u_{axi}}}{u'\sqrt{2}} \right) \right) \tag{5}$$

According to the literature, other methodologies have been proposed in order to build ignition probability map using RANS. For example, [4] used a Lagrangian approach to compute the flame kernel trajectory and predicted the latter quenching of the kernel using a Karlovitz number. This methodology doesn't introduce simulation of the early phase of energy deposit, still it seems to capture some features of experimental ignition mapping quite well. Another similar approach has been tested [3], using LES to build an ignition probability map, allowing to capture the unstationary effects. Following these works, the improvements of our methodology could be done, modeling more accurately the flame kernel trajectory as well as the effect of flow unsteadiness.

4. Results and discussion

4.1. Ignition mapping

The methodology described in Section 3.2 has been applied to the RANS stationary flow field. Duration of each ignition simulation is set to 1 ms, according to high speed visualizations, in order to verify the hypothesis of kernel immobility. Fig. 9 shows the successive steps to identify locations with good ignition probability. The analysis of the kernel temperature (Condition 3) is not shown here, because kernel temperature $\geqslant 2600$ K in the whole area tested, so remains above stoechiometric flame temperature. This criterion is more relevant with low-temperature flow, for which heat transfer from the kernel to its surrounding is stronger. For current case, only Conditions 1, 2 and 4 are analyzed.

On Fig. 9.a, it can be seen the separation between the kernel with local inflammation detection. Fig. 9.b shows the growth of the ignition kernel after the ignition simulation. Ignition and kernel growth are possible in region with strong liquid concentration, on the spray cone and in the vicinity of the wall. After impact of the spray on the wall, part of the droplets is recirculated by the flow in the lateral zone. The gas flow also exhibits a central recirculation zone, but droplets recirculation in this zone doesn't provide enough fuel to enable ignition. The upstream propagation probability is drawn on Fig. 9.c. Two zones of low P_{up} can be identified: one corresponds to the high velocity zone of the jet, the other is located near the wall, downstream from $z = 80$ mm abscissa.

Finally, Fig. 9.d shows a scatter plot of ignition kernels allowing ignition of the combustor. The different criteria have been combined, using the following threshold: $P_{up} \geqslant 0.6$, $r/r_1 \geqslant 1.15$. The threshold level on P_{up} insures that $S_T > \overline{u_{axi}}$. It shall be noticed that the choice of threshold levels impacts greatly on the results of the elimination, and can be discussed. Numerical results match well with experimental ignition data. Ignition is favored inside the lateral recirculation zone, with negative $\overline{u_{axi}}$ and adequate local equivalence ratio.

For abscissa $z = 116$ mm, some kernel with successful ignition can be found near the wall, but P_{up} remains lower than that inside the recirculation zone, and this region is less favorable to ignition success. Actually, high speed visualization of the ignition process showed the formation and growth of an ignition kernel in this zone. It seems to indicate that the limiting criterion for ignition success is the flame kernel propagation rather than the formation of the kernel.

It shall be noticed that the exact ignition probability is not reproduced by the ignition mapping, since P_{up} is only calculated at the spark discharge location, and doesn't take into account complete trajectory and possible later quenching of the kernel. Still, it is possible to isolate some zones where combustor ignition is possible, and to understand some limiting parameters to the phenomena.

4.2. Flame propagation

In the present work, flame propagation has been tested only with RANS. The CRAMER model has been chosen to model the turbulent flame [13]. This model is suited for the simulation of premixed or partially premixed flame, with the

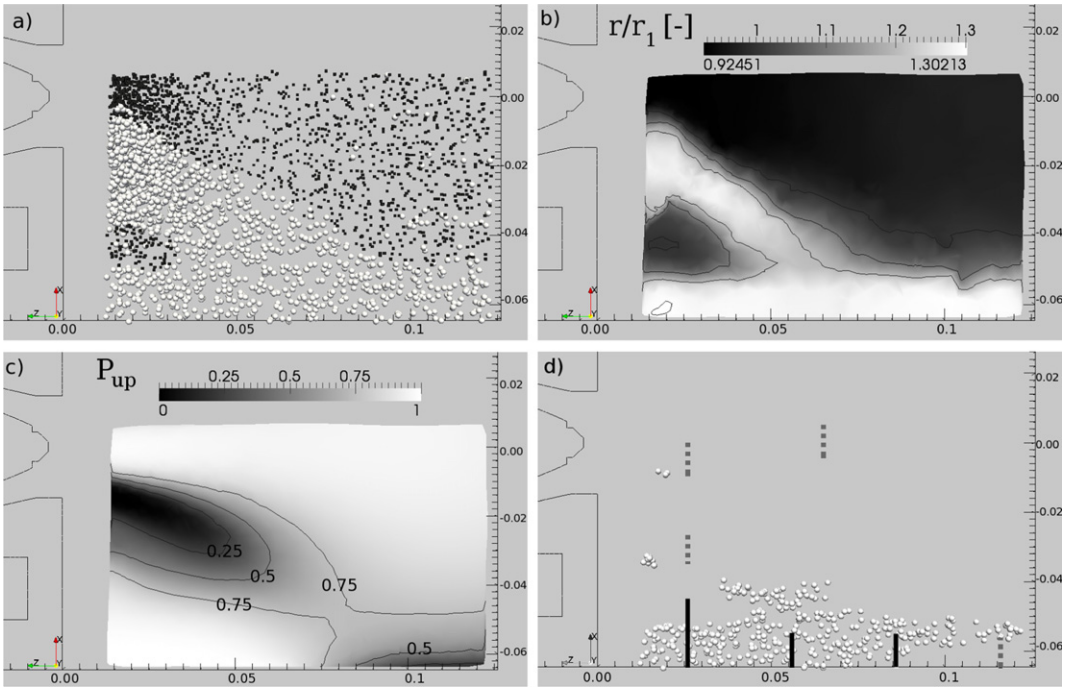

Fig. 9. Ignition probability mapping on MERCATO: a) ignition spheres scatter plot (■ = local ignition failure, ○ = local ignition success); b) kernel growth; c) upstream flame propagation probability P_{up} with iso-contour; d) scatter plot of successful global ignition positions from simulation, and experimental results (– = combustor ignition, ··· = no-ignition).

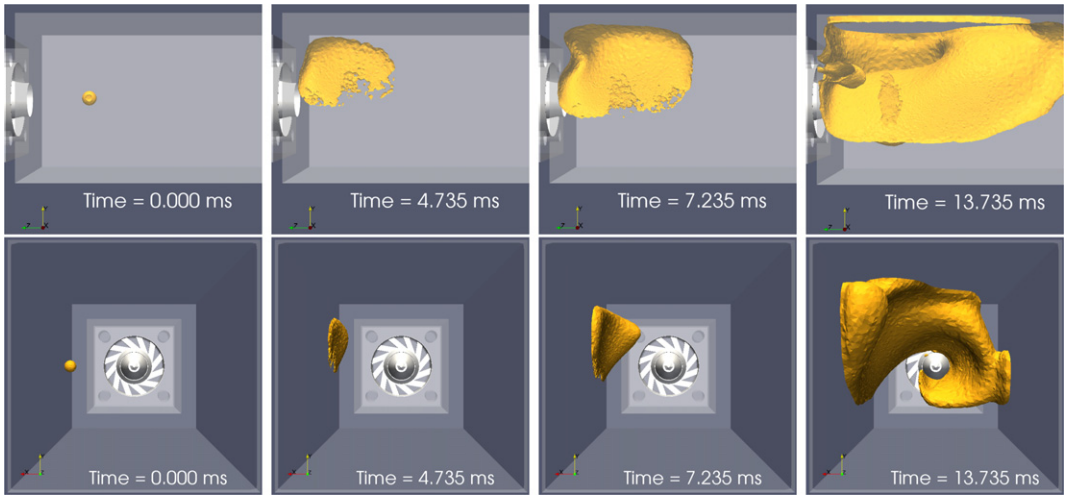

Fig. 10. Simulation of the kernel propagation for spark plug at position $z = 56$ mm (temperature iso-contour $T = 1300$ K).

assumption of infinity fast chemistry. From a steady flow solution, initial conditions for the kernel are extracted, ignition simulation is performed. Then, final state of the kernel is used to initiate the flame propagation simulation.

Figs. 10 and 11 show snapshots from the two unsteady RANS flame propagations. For an energy deposit at $z = 56$ mm, the hot kernel is convected and trapped inside the lateral recirculation zone, then grows until the flame can reach the spray. After around 10 ms, the hot gas volume wraps around the axis of the injection system, at the limit of the central recirculation zone. The flame propagation follows the swirl, which has been experimentally observed during ignition tests [7]. It has to be noticed that the delay of the flame propagation seems to be underestimated in our simulation.

For an energy deposit at $z = 116$ mm position, the flame kernel generation is also possible, but upstream propagation of the kernel is prevented by the topology of the gas velocity field. The volume of hot gas expands downstream from the jet, and the flame fails to anchor to the injector nozzle. Without this condition, the flame cannot sustain into the combustor.

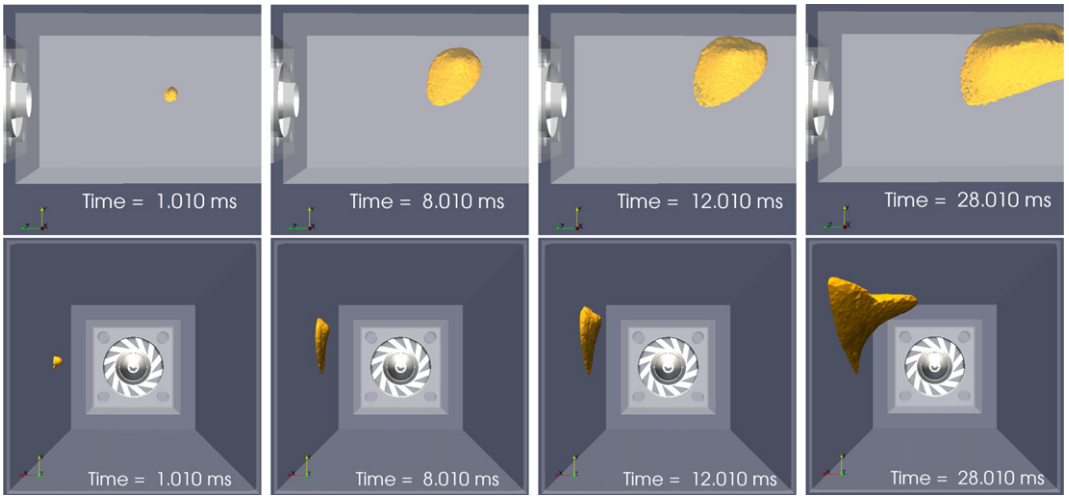

Fig. 11. Simulation of the kernel propagation for spark plug at position $z = 116$ mm (temperature iso-contour $T = 1300$ K).

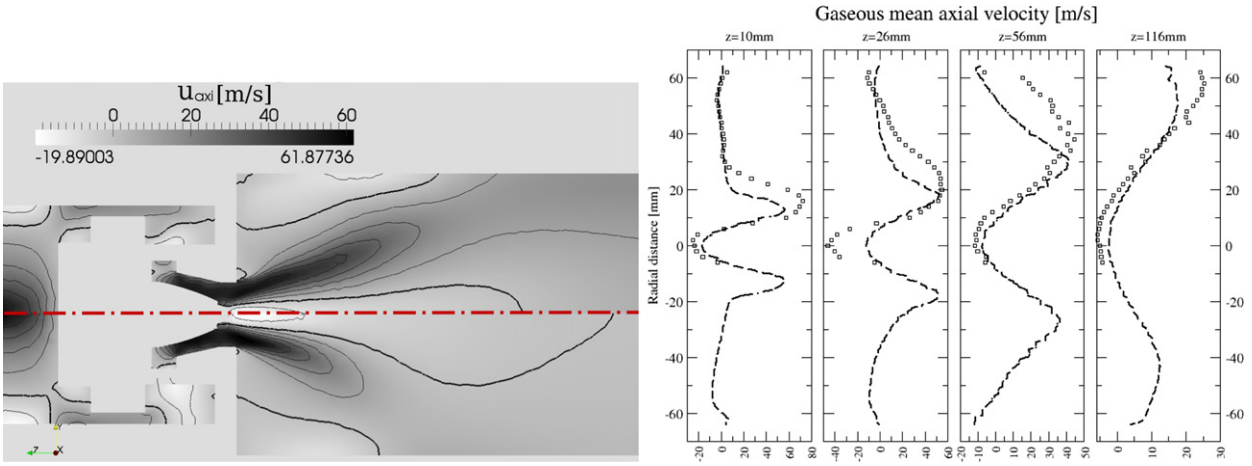

Fig. 12. Left: comparison of RANS axial gas velocity for reactive (upper half) and non-reactive flow (lower half), iso-lines (bold = recirculation zones limits). Right: axial gas velocity profile for reactive flow (□ = PDA, -- = RANS).

For several cases, visualizations of the kernel showed that the kernel is convected downstream and upward, following the swirl. This trend is also reproduced by unsteady RANS (see Fig. 11).

4.3. Stabilized reactive flow

The successful ignition simulation has been running until convergence, in order to obtain stabilized reactive flow field. The axial gas velocity profiles have been compared to the one from non-reactive RANS and from PDA measurements for reactive flow (see Fig. 12). Compared to non-reactive flow, the change of density caused by heating increases the maximum axial velocity. The length and maximum width of the axial recirculation zone are diminished. Some discrepancies are observed with experimental results. The widening of the jet observed on $z = 26$ and 56 mm sections is not reproduced by RANS. For $z = 10$ mm section, maximum velocity of the jet is underestimated, as the velocity levels inside the central recirculation zone, which vary little from cold flow case.

The absence of modeling for the large scale could be responsible for uncorrect prediction of the mixing of hot products and underestimation of the gas temperature inside the recirculation zone. The injection of droplets at ambient temperature, far from the injector nozzle, could also displace the real location of the flame front. Complementary investigations are needed to improve the agreement for RANS reactive flow predictions.

5. Conclusions and perspectives

RANS and LES have been applied to simulate non-reactive two-phase flow of an experimental combustor, with Lagrangian modeling for the liquid phase. The steady flow is well reproduced by both methods, and LES enabled to capture precisely the hydrodynamic instability present for this regime.

From RANS results, ignition mapping and unsteady flame propagation have been tested, and results showed good agreements with the main features observed on the combustor during ignition tests. For stabilized combustion regime, some works are still necessary to improve agreement between RANS and experimental data. Both approaches have to be tested with LES. The modeling of large scale should improve the accuracy of the results, in term of ignition probability prediction.

Acknowledgements

The authors would like to acknowledge the financial support from Turbomeca, the “Association nationale pour la recherche et la technologie” and the “Direction générale de l’armement”.

References

[1] M. Thiele, S. Selle, U. Riedel, J. Warnatz, U. Maas, Numerical simulation of spark ignition including ionization, Proceedings of the Combustion Institute 28 (2000) 1177–1185.
[2] V. Subramanian, P. Domingo, L. Vervisch, Large eddy simulation of forced ignition of an annular bluff-body burner, Combustion and Flame 157 (2010) 579–601.
[3] J. Weckering, A. Sadiki, J. Janickay, E. Mastorakos, Investigations of ignition probability of a forced ignited turbulent methane jet using LES, in: V European Conference on Computational Fluid Dynamics, Lisbon, June 2010.
[4] A. Neophytou, Spark ignition and flame propagation in sprays, PhD thesis, University of Cambridge, 2010.
[5] N. Garcia Rosa, P. Villedieu, J. Dewitte, G. Lavergne, A new droplet wall interaction model, in: Proceedings of the ICLASS, Kyoto, August 2006.
[6] R. Lecourt, G. Linassier, G. Lavergne, Detailed characterisation of a swirled air/kerosene spray in reactive and non-reactive conditions downstream from an actual turbojet injection system, in: Proceedings of ASME Turbo Expo 2010, Vancouver, Canada, June 2011.
[7] A. Lang, R. Lecourt, F. Guliani, Statistical evaluation of ignition phenomena in turbojet engines, in: Proceedings of ASME Turbo Expo 2010, Glasgow, June 2010.
[8] S. Pascaud, Vers la simulation aux grandes échelles des écoulements turbulents diphasiques réactifs : application aux foyers aéronautiques, PhD thesis, Université de Toulouse, 2006.
[9] N. Syred, A review of oscillation mechanisms and the role of the precessing vortex core (PVC) in swirl combustion systems, Progress in Energy and Combustion Science 32 (2006) 93–161.
[10] N. García Rosa, G. Linassier, R. Lecourt, P. Villedieu, G. Lavergne, Experimental and numerical study of high-altitude ignition of a turbojet combustor, in: Heat Transfer Engineering, Xi’an, 2009.
[11] B. Franzelli, E. Riber, M. Sanjose, T. Poinsot, A two-step chemical scheme for large eddy simulation of kerosene–air flames, Combustion and Flame 157 (2010) 1364–1373.
[12] G. Damkoler, NACA Technical Memorandum No. 1112, 1947.
[13] R. Borghi, M. Champion, Modélisation et théorie des flammes, Éditions TECHNIP, 2000.